



**HAL**  
open science

# Rib Waveguide Plasmonic Sensor for Lab-on-Chip Technology

Daniel Almeida, João Costa, Alessandro Fantoni, Manuela Vieira

► **To cite this version:**

Daniel Almeida, João Costa, Alessandro Fantoni, Manuela Vieira. Rib Waveguide Plasmonic Sensor for Lab-on-Chip Technology. 13th Doctoral Conference on Computing, Electrical and Industrial Systems (DoCEIS), Jun 2022, Caparica, Portugal. pp.187-196, 10.1007/978-3-031-07520-9\_17 . hal-04308382

**HAL Id: hal-04308382**

**<https://inria.hal.science/hal-04308382>**

Submitted on 27 Nov 2023

**HAL** is a multi-disciplinary open access archive for the deposit and dissemination of scientific research documents, whether they are published or not. The documents may come from teaching and research institutions in France or abroad, or from public or private research centers.

L'archive ouverte pluridisciplinaire **HAL**, est destinée au dépôt et à la diffusion de documents scientifiques de niveau recherche, publiés ou non, émanant des établissements d'enseignement et de recherche français ou étrangers, des laboratoires publics ou privés.



Distributed under a Creative Commons Attribution 4.0 International License



This document is the original author manuscript of a paper submitted to an IFIP conference proceedings or other IFIP publication by Springer Nature. As such, there may be some differences in the official published version of the paper. Such differences, if any, are usually due to reformatting during preparation for publication or minor corrections made by the author(s) during final proofreading of the publication manuscript.

# Rib Waveguide Plasmonic Sensor for Lab-On-Chip Technology

Daniel Almeida<sup>1,2,3</sup>, João Costa<sup>2,3</sup>, Alessandro Fantoni<sup>2,3</sup>, Manuela Vieira<sup>1,2,3</sup>

<sup>1</sup>School of Science and Technology, NOVA University of Lisbon, Caparica, Portugal

<sup>2</sup>UNINOVA-CTS, Caparica, Portugal

<sup>3</sup>ISEL - Instituto Superior de Engenharia de Lisboa, Instituto Politécnico de Lisboa, Lisboa, Portugal

dg.almeida@campus.fct.unl.pt

{jcosta, afantoni}@deetc.isel.ipl.pt

mv@isel.ipl.pt

**Abstract.** A prompt medical diagnosis is of major importance, starting the appropriate treatment earlier results in better outcomes and faster recovery times. Plasmonic biosensors based on photonic integrated circuits (PIC) are potential candidates in the development of lab-on-chip (LOC) technology, allowing digitalization of results and virtualization of laboratorial procedures in the detection of important biomarkers. These sensors have the advantages of high sensitivity and faster analysis when compared with traditional laboratorial methodologies. We study the possibility of exciting a surface plasmon, using low-cost fabrication methods and techniques based on amorphous silicon compounds, rib waveguide geometry and dimensions compatible with plasma-enhanced chemical vapor deposition (PECVD) and ultraviolet (UV) lithography. Results of Finite-Difference Time-Domain (FDTD) simulation of the plasmon excitation and sensor response are presented and discussed.

**Keywords:** Plasmonics, Lab-on-chip, Amorphous silicon, Photonic integrated circuit.

## 1 Introduction

Clinical assays are fundamental diagnostic tools employed to detect disease markers on samples of human tissue and fluids. Conventional techniques require expensive laboratory equipment and trained personnel, making the process complex, expensive and time-consuming. Lab-on-chip (LOC) technology, based on compact optical devices, such as photonic integrated circuit (PIC) biosensors, can be designed to detect several biomarkers (e.g. proteins, nucleic acids, drugs, pathogens and human cells) [1], paving the way to the development of Point-of-Care (PoC) diagnostic platforms. Studies demonstrate that these highly integrated sensors can be employed in the diagnosis of several diseases and health conditions, such as viruses [2], cancers [3] and acute kidney injury [4]. Early biomarker detection contributes to improving patient prognosis. State-of-the-Art photonic biosensors are able to detect analytes in a few

minutes [5] and can achieve very high sensitivities [1], with detection limits between  $10^{-4}$  and  $10^{-6}$  RIU (refractive index units) or even less [1, 6–8].

The success of PoC testing platforms is dependent on the development of technologies which are easily adapted to the detection of various analytes with high sensitivity and suitable for low-cost large scale deployment. Surface Plasmon Resonance sensors based on the Kretschmann configuration [9] are an example of a technology which excels on sensitivity and adaptability to different analytes. On the negative side, the equipment is too expensive and bulky for mass deployment in PoC applications. There is much interest in solutions that avoid large or expensive components, such as motor rotation stages and prisms, and which are based on low-cost materials and fabrication processes. In recent studies a large diversity of photonic sensor architectures comprising waveguides have been reported, the vast majority of sensors lay inside one of the following categories: 1) Plasmonic sensors based solely on waveguides [10–12]; 2) Interferometric sensors, Fig. 1, exploring surface plasmon resonance [13–15], the evanescent wave effect [16] or the interference between two modes (bimodal waveguides) [17]; 3) Sensors employing one or more ring resonators [18, 19], Fig. 1; 4) Sensors featuring cavities [20, 21].

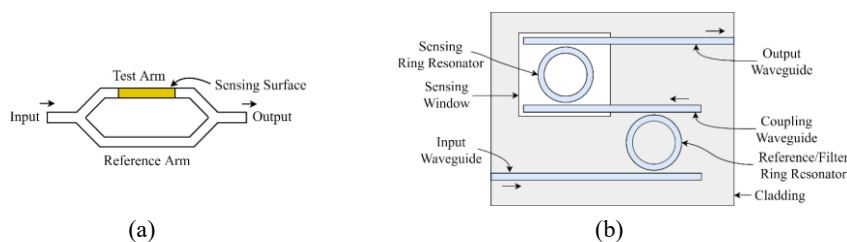


**Fig. 1.** Top view of two photonic sensor configurations (simplified). (a) Mach-Zehnder Interferometer (MZI) implementation based on waveguides, comprising Y-junction splitter and combiner. (b) An example of ring resonator topology, the Vernier-cascade sensor [22], this configuration comprises three waveguides and two ring resonators, the filter ring resonator and input waveguide are totally covered by the cladding.

The trend has been to reduce the form factor of the photonic circuits, to achieve higher integration, leveraged by sub-micrometer lithographic processes [19, 21, 23–25], however, there is a major drawback in size reduction, which are the increased manufacturing costs. A possible alternative are larger photonic devices, which can be produced at lower costs [26]. Despite current trends, multi-micron sensor devices have been proposed in the last decade [16, 17], these designs are based on rib waveguides. Considering the State-of-the-Art in biosensing, the following research question is proposed:

- What could be a suitable method to develop a low-cost, highly sensitive, compact and efficient sensor system that can be suitable to the detection of various biomarkers in point-of-care medical applications?

Sub-micron waveguides have the advantage of higher integration, however, when compared with multi-micron waveguides, the former have the disadvantages of higher losses and higher sensitivity to fabrication imperfections [26]. Multi-micron waveguides can be fabricated using low-cost processes with lower spatial resolutions,

such as Plasma-Enhanced Chemical Vapor Deposition (PECVD) combined with ultraviolet (UV) lithography. Multi-micron rib waveguides have some advantages when compared with other waveguide types (e.g. strip waveguides), in terms of light coupling efficiency, losses and production costs, making them suitable for biosensing applications [16]. Large cross-section rib waveguides can be designed to support single-mode (SM) operation [27–29], resulting in reduced light coupling loss when interfaced with optical fibers [30] and lower losses due to side-wall roughness [31].

Hydrogenated amorphous silicon (a-Si:H) and its compounds, hydrogenated amorphous silicon carbide (a-SiC:H) and hydrogenated amorphous silicon nitride (a-SiN:H), can be deposited by PECVD at lower temperatures (typically, between 200 °C - 400 °C) [32], reducing fabrication costs. By controlling the compound percentages, it is possible to fine tune the material structure and optical properties, like for example the refractive index [33], allowing the integration of several components, such as power splitters, interferometers, waveguides and photodetectors.

In this research, finite-difference time-domain (FDTD) and Finite Element Method (FEM) simulations are performed to study a SM rib waveguide surface plasmon resonance sensor. The photonic circuit is of low complexity and can be fabricated with inexpensive materials, such as silicon dioxide (SiO<sub>2</sub>) and nitrogen-rich a-SiN:H, the sensitive layer is made of a thin silver layer (Ag), with 40 nm thickness. The device can be fabricated using low-cost methods such as PECVD and UV lithography, also benefiting from better light coupling efficiency, due to its larger cross-section. The operating wavelength is 405 nm, the same used in high-definition optical discs, in the limit of the visible spectrum.

## 2 Contribution to Technological Innovation for Digitalization and Virtualization

Industry 4.0 is a concept devised to the industrial domain, comprising individualization and virtualization [34], implemented by new technologies for automation and data exchange. This concept applied to the health domain is called Health 4.0 [35]. The six principles of Industry 4.0 [34] are: 1) Interoperability; 2) Virtualization; 3) Decentralization; 4) Real-Time Capability; 5) Service Orientation; 6) Modularity. Biosensors and LOC technology contribute to all seven principles of Health 4.0:

Interoperability can be achieved by aggregation and integration of the different devices and services, being a major step towards the generation of meaningful information [35]. Data fusion combines information collected from different sensors to more accurately assess the patient's health conditions [36], helping medical staff in the establishment of a personalized treatment.

With point-of-care analytical platforms, the clinical assay procedure can be partially virtualized, because the laboratory is “contained within a single device” and result interpretation can be made by computational algorithms, contributing to a significant reduction of the workload and the physical size of the lab.

Decentralization is accomplished due to the portability of the LOC platform, enabling clinical assays to be conducted *in-loco*, by a single doctor, nurse or analyst,

the service is personalized, meaning healthcare can shift from centralized to a customized patient-oriented service.

Biosensors are extremely fast and typically can provide results within minutes [5], significantly contributing for real-time diagnosis. Due to the increased access to clinical assays, appropriate disease follow-up and prevention measures can be taken, so the probability of serious episodes and hospital admission lowers significantly.

The sensors' output is converted into the digital domain, allowing interfacing with latest generation networks (i.e. 5G) and cloud technologies, which are enablers for service orientation in the health domain [35]. The concept of modularity is also applicable to PoC equipment for medical assays, considering that the equipment features one or more receptacles where biosensor "cartridges" can be inserted or removed. Following this approach, LOCs can adapt to detect different analytes, the sensor "cartridges" can also be periodically upgraded or replaced if malfunctioning.

Another principle was added later: Safety, security and resilience [35]. In order to minimize the risks for the patients, it is important to assure the reliability and resilience of the system, by improving the biosensor's sensitivity and selectivity.

Conventional medical diagnostics rely primarily on the symptomatology, being prone to fail due to inadequate reporting or lack of symptoms on initial stages of disease [36]. Machine learning (ML), artificial intelligence (AI) and the internet of things (IoT) have the potential to be applied with biosensors, allowing real-time monitoring [37].

### 3 Theoretical Background and Sensor Configuration

The sensor developed in this study is based on a SM silicon-on-insulator (SOI) rib waveguide, having an a-SiN:H core deposited over a SiO<sub>2</sub> substrate, Fig. 2. The plasmonic section is covered by a thin silver (Ag) layer. It differs from the work of Fantoni *et al.* [12], because it is focused on a multi-micron design, made possible by a rib geometry, different waveguide materials and operating wavelength.

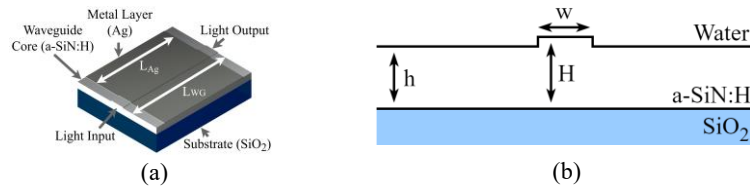


**Fig. 2.** Sensor design based on the rib waveguide. (a) Tridimensional model,  $L_{WG}$  and  $L_{Ag}$  represent waveguide and silver layer lengths, respectively. (b) Transversal section,  $w$  represents rib width,  $H$  rib height and  $h$  slab height.

#### 3.1 Single-Mode Rib Waveguide Dimensioning

It is desirable to design waveguides for SM propagation in order to maximize power efficiency. Rib waveguide SM operation was the focus of several studies [27–29]. Rib waveguide geometry is characterized by three main parameters, rib width ( $w$ ), rib

height ( $H$ ) and slab height ( $h$ ), Fig. 2. To guarantee the design is compatible with low-cost lithographic and deposition processes (UV and PECVD), the width of the rib ( $w$ ) should be equal to or greater than  $1 \mu\text{m}$ , so it was set at  $1.5 \mu\text{m}$ , to allow a small margin. Etch depth ( $D$ ) was defined as  $0.1 \mu\text{m}$ , the maximum  $r$  value was set at  $0.9$ . Expression (1) establishes the relationship between rib waveguide design parameters and SM operation [28, 29], the expression is valid for  $0.5 \leq r < 1$ . By replacing  $h$  in  $r = h/H$  by  $H - D$ , the rib height ( $H$ ) can be obtained from (1):

$$w/H \leq \alpha + r \cdot (1 - r^2)^{-1/2}. \quad (1)$$

Parameter  $\alpha$  is 0 when considering the Effective Index Method (EIM), Pogossian *et al.* [28] or 0.3 according to Soref *et al.* [27]. Following the more conservative approach of null  $\alpha$ , the resulting rib height value is  $0.82 \mu\text{m}$ , implying a slab height value of  $0.72 \mu\text{m}$ , which were the dimensions used in this study.

### 3.2 Surface Plasmon Polariton (SPP) Excitation

Surface Plasmon Polaritons can only be excited by TM guided modes. In order to excite the SPP the effective refractive index difference between the plasmonic mode and the waveguide fundamental TM mode must be small. SPP complex refractive index as a function of angular frequency is given by (2):

$$n_{\text{effSPP}}(\omega) = \sqrt{\frac{\varepsilon_d(\omega) \varepsilon_m(\omega)}{\varepsilon_d(\omega) + \varepsilon_m(\omega)}}, \quad (2)$$

where  $\omega$  is the angular frequency in rad/s,  $\varepsilon_d(\omega)$ ,  $\varepsilon_m(\omega)$  correspond to the complex permittivity function of the sample medium and metal, respectively.

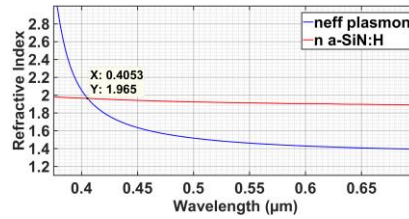


**Fig. 3.** Effective refractive index of the SPP (real component), represented in blue, refractive index of a-SiN:H with  $\text{Si}/\text{N} < 1$  (real component), represented in red. The intersection point shows an ideal SPP excitation wavelength of 405 nm and a refractive index of 1.965.

From (2) and considering that the effective refractive index of the waveguide's fundamental mode is similar to the index of the core material, the intersection point is found in Fig. 3. The resulting wavelength of 405.3 nm is ideal to excite the SPP from the fundamental TM mode of the waveguide. Results assume the sample medium is water, the metal layer is silver (refractive index from Jiang *et al.* [38]) and the waveguide material is a-SiN:H with Si/N ratio under 1 (refractive index from Charifi *et al.* [39]). The intersection point occurs for a refractive index of 1.965.

## 4 Results

### 4.1 Modal Analysis

In Fig. 4, the major electric and magnetic XY field distributions are depicted, on the top of the rib a small field intensity is present, this effect makes plasmon excitation possible. The mode's effective refractive index is 1.949, the extinction coefficient is  $2.8 \times 10^{-12}$ , because the material is considered non-dispersive.

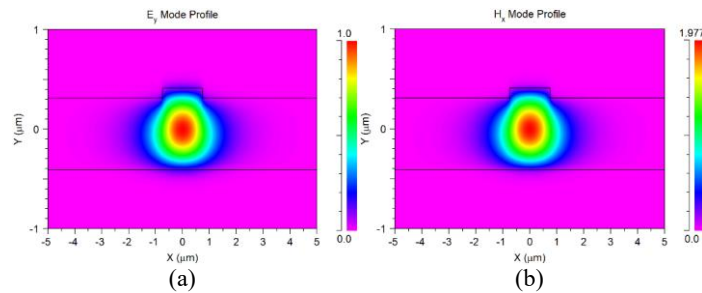


**Fig. 4.** Fundamental TM mode of the rib waveguide obtained in FEM simulation. (a)  $E_y$  and (b)  $H_x$  fields. Layers are delimited by black lines (from top to bottom, water, a-SiN:H and  $\text{SiO}_2$ ).

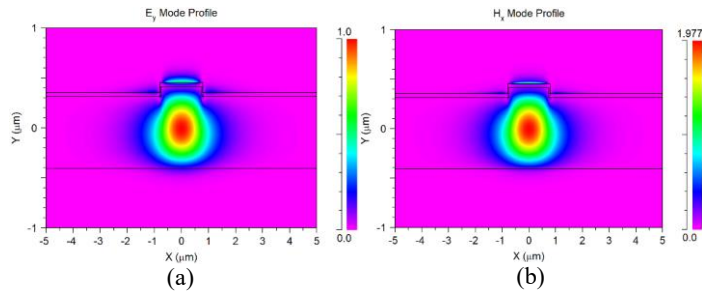


**Fig. 5.** FEM simulation results of the coupling between the fundamental TM mode and the SPP. (a)  $E_y$  and (b)  $H_x$  fields. Layers are delimited by black lines (from top to bottom, water, silver, a-SiN:H and  $\text{SiO}_2$ ).

In Fig. 5, it is possible to notice the coupling between the fundamental TM mode of the rib waveguide and the surface plasmon mode, in this region of the sensor a thin silver layer with 40 nm thickness is deposited over the waveguide's core. The plasmonic field is visible over the center of the silver layer placed on top of the waveguide's rib. The effective refractive index of the mode is approximately 1.948. The deviation from the predicted refractive index of 1.965 (Fig. 3) is under 0.9 %.

In Fig. 6, the vertical cuts of the major electric and magnetic fields are represented, the higher peaks represent the waveguide fundamental TM mode, which is confined within the waveguide's core. Minor peaks are also visible, which correspond to the SPP propagating over the silver layer.



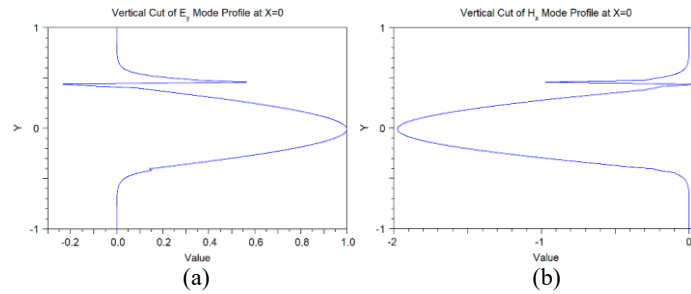


**Fig. 6.** Vertical cut of: (a)  $E_y$  and (b)  $H_x$  fields, the characteristic plasmon field profile is present on the top, showing coupling between the waveguide TM mode and SPP mode.

#### 4.2 Sensor's Response

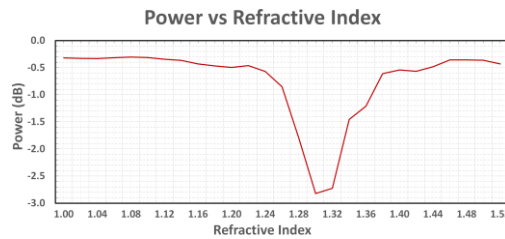


**Fig. 7.** Transmitted power as a function of the sample medium refractive index.

The sensor's response was simulated for a waveguide length ( $L_{WG}$ ) of  $12 \mu\text{m}$  and a silver layer length ( $L_{Ag}$ ) of  $10 \mu\text{m}$ , Fig. 2. FDTD simulations were performed for sample medium refractive index values between 1 and 1.52. The fundamental TM mode is coupled to the input of the waveguide and power is measured at the output.

In Fig. 7, for refractive index values between 1.29 and 1.31, a large dip is observable in the sensor's response, output power is under  $-2.7 \text{ dB}$ , confirming the sensing behavior. The attenuation from the baseline is  $2.2 \text{ dB}$ .

## 5 Conclusions and Future Work

A plasmonic sensor based on a rib waveguide was designed and simulated. The waveguide geometry and multi-micron size allows light coupling from optical fibers, requiring only a plane-convex lens termination to converge the light beam. Due to the large size of the sensor, simple design and constituting materials (a-SiN:H), low-cost fabrication techniques can be employed, such as PECVD and UV lithography.

The sensitivity window covers the refractive index of human body fluids making it interesting to biosensing platforms. The dip in the power of the transfer function is still

modest leaving room for improvement. Since the sensor operates with visible light (405nm), testing is facilitated. This wavelength is also used in high-definition optical disks. Further studies are necessary to establish the optimal metal and waveguide lengths. Equally important is the impact of the silicon-to-nitrogen ratio of a-SiN:H. Discovering the ideal proportion is fundamental to achieve the best plasmon excitation scenario. It is also necessary to improve the a-SiN:H model with  $k$  values based on experiments conducted at visible light wavelengths (400 nm to 700 nm).

**Acknowledgments.** Research supported by FCT - Fundação para a Ciência e Tecnologia, through grant SFRH/BD/07792/2021 and projects PTDC/NAN-OPT/31311/2017, FCT/MCTES: UIDB/00066/2020, and by Instituto Politécnico de Lisboa, through project IPL/2021/wavesensor\_ISEL.

## References

1. Kazanskiy, N.L., Khonina, S.N., Butt, M.A., Kaźmierczak, A., Piramidowicz, R.: State-of-the-art optical devices for biomedical sensing applications—a review. *Electron.* 10, 1–29 (2021). <https://doi.org/10.3390/electronics10080973>
2. Shrivastav, A.M., Cvelbar, U., Abdulhalim, I.: A comprehensive review on plasmonic-based biosensors used in viral diagnostics. *Commun. Biol.* 4, 1–12 (2021). <https://doi.org/10.1038/s42003-020-01615-8>
3. Soler, M., Estevez, M.C., Villar-Vazquez, R., Casal, J.I., Lechuga, L.M.: Label-free nanoplasmonic sensing of tumor-associate autoantibodies for early diagnosis of colorectal cancer. *Anal. Chim. Acta.* 930, 31–38 (2016). <https://doi.org/10.1016/j.aca.2016.04.059>
4. Albeltagy, E.S., Abdul-Mohymen, A.M., Taha, D.R.A.: Early diagnosis of acute kidney injury by urinary YKL-40 in critically ill patients in ICU: a pilot study. *Int. Urol. Nephrol.* 52, 351–361 (2020). <https://doi.org/10.1007/s11255-019-02364-2>
5. Soler, M., Huertas, C.S., Lechuga, L.M.: Label-free plasmonic biosensors for point-of-care diagnostics: a review. *Expert Rev. Mol. Diagn.* 19, 71–81 (2019). <https://doi.org/10.1080/14737159.2019.1554435>
6. Soler, M., Lechuga, L.M.: Principles, technologies, and applications of plasmonic biosensors. *J. Appl. Phys.* 129, (2021). <https://doi.org/10.1063/5.0042811>
7. Diao, B., Wen, K., Chen, J., Liu, Y., Yuan, Z., Han, C., Chen, J., Pan, Y., Chen, L., Dan, Y., Wang, J., Chen, Y., Deng, G., Zhou, H., Wu, Y.: Diagnosis of acute respiratory syndrome coronavirus 2 infection by detection of nucleocapsid protein. *medRxiv.* (2020). <https://doi.org/10.1101/2020.03.07.20032524>
8. Gauglitz, G.: Critical assessment of relevant methods in the field of biosensors with direct optical detection based on fibers and waveguides using plasmonic, resonance, and interference effects. *Anal. Bioanal. Chem.* 412, 3317–3349 (2020). <https://doi.org/10.1007/s00216-020-02581-0>
9. Kretschmann, E., Raether, H.: Radiative decay of nonradiative surface plasmons excited by light. *Z Naturforsch A.* 23, 2135–6 (1968)
10. Yuan, D., Dong, Y., Liu, Y., Li, T.: Design of a high-performance micro integrated surface plasmon resonance sensor based on silicon-on-insulator rib waveguide array. *Sensors (Switzerland).* 15, 17313–17328 (2015). <https://doi.org/10.3390/s150717313>
11. Jabbarzadeh, F., Habibzadeh-Sharif, A.: High performance dielectric loaded graphene plasmonic waveguide for refractive index sensing. *Opt. Commun.* 479, 126419 (2021). <https://doi.org/10.1016/j.optcom.2020.126419>

12. Fantoni, A., Costa, J., Fernandes, M., Vygranenko, Y., Vieira, M.: Theory and FDTD simulations of an amorphous silicon planar waveguide structure suitable to be used as a surface plasmon resonance biosensor. *Opt. Pura y Apl.* 53, 1–8 (2020). <https://doi.org/10.7149/OPA.53.2.51032>
13. da Lee, E., Lee, Y.J., Shin, E., Kwon, S.H.: Mach-Zehnder interferometer refractive index sensor based on a plasmonic channel waveguide. *Sensors (Switzerland)*. 17, 12–16 (2017). <https://doi.org/10.3390/s17112584>
14. Lotfi, F., Sang-Nourpour, N., Kheradmand, R.: High-sensitive plasmonic sensor based on Mach-Zehnder interferometer. *Opt. Laser Technol.* 137, 106809 (2021). <https://doi.org/10.1016/j.optlastec.2020.106809>
15. Gupta, R., Labella, E., Goddard, N.J.: An optofluidic Young interferometer sensor for real-time imaging of refractive index in  $\mu$ TAS applications. *Sensors Actuators, B Chem.* 321, 128491 (2020). <https://doi.org/10.1016/j.snb.2020.128491>
16. Yuan, D., Dong, Y., Liu, Y., Li, T.: Mach-Zehnder interferometer biochemical sensor based on silicon-on-insulator rib waveguide with large cross section. *Sensors (Switzerland)*. 15, 21500–21517 (2015). <https://doi.org/10.3390/s150921500>
17. Jung, H.: Modal analysis and design of silicon nitride rib waveguides for evanescent-wave bimodal biosensors. *Curr. Opt. Photonics*. 3, 382–389 (2019). <https://doi.org/10.3807/COPP.2019.3.5.382>
18. Butt, M.A., Khonina, S.N., Kazanskiy, N.L.: Plasmonic refractive index sensor based on metal–insulator–metal waveguides with high sensitivity. *J. Mod. Opt.* 66, 1038–1043 (2019). <https://doi.org/10.1080/09500340.2019.1601272>
19. Chou Chao, C.T., Chou Chau, Y.F., Chiang, H.P.: Highly sensitive metal-insulator-metal plasmonic refractive index sensor with a centrally coupled nanoring containing defects. *J. Phys. D. Appl. Phys.* 54, (2021). <https://doi.org/10.1088/1361-6463/abce7f>
20. Rakhshani, M.R., Mansouri-Birjandi, M.A.: High-Sensitivity Plasmonic Sensor Based on Metal-Insulator-Metal Waveguide and Hexagonal-Ring Cavity. *IEEE Sens. J.* 16, 3041–3046 (2016). <https://doi.org/10.1109/JSEN.2016.2522560>
21. Luo, S., Li, B., Xiong, D., Zuo, D., Wang, X.: A High Performance Plasmonic Sensor Based on Metal-Insulator-Metal Waveguide Coupled with a Double-Cavity Structure. *Plasmonics*. 12, 223–227 (2017). <https://doi.org/10.1007/s11468-016-0253-y>
22. Martens, D., Bienstman, P.: Comparison between Vernier-cascade and MZI as transducer for biosensing with on-chip spectral filter. *Nanophotonics*. 6, 703–712 (2017). <https://doi.org/10.1515/nanoph-2016-0181>
23. Rahmatiyar, M., Danaie, M., Afsahi, M.: Employment of cascaded coupled resonators for resolution enhancement in plasmonic refractive index sensors. *Opt. Quantum Electron.* 52, 1–19 (2020). <https://doi.org/10.1007/s11082-020-02266-z>
24. Butt, M.A., Kazanskiy, N.L., Khonina, S.N.: Highly integrated plasmonic sensor design for the simultaneous detection of multiple analytes. *Curr. Appl. Phys.* 20, 1274–1280 (2020). <https://doi.org/10.1016/j.cap.2020.08.020>
25. Danaie, M., Shahzadi, A.: Design of a High-Resolution Metal–Insulator–Metal Plasmonic Refractive Index Sensor Based on a Ring-Shaped Si Resonator. *Plasmonics*. 14, 1453–1465 (2019). <https://doi.org/10.1007/s11468-019-00926-9>
26. Zilkie, A.J., Srinivasan, P., Trita, A., Schrans, T., Yu, G., Byrd, J., Nelson, D.A., Muth, K., Lerose, D., Alalusi, M., Masuda, K., Ziebell, M., Abediasl, H., Drake, J., Miller, G., Nykanen, H., Kho, E., Liu, Y., Liang, H., Yang, H., Peters, F.H., Nagra, A.S., Rickman, A.G.: Multi-micron silicon photonics platform for highly manufacturable and versatile photonic integrated circuits. *IEEE J. Sel. Top. Quantum Electron.* 25, (2019). <https://doi.org/10.1109/JSTQE.2019.2911432>

27. Soref, R.A., Schmidtchen, J., Petermann, K.: Large Single-Mode Rib Waveguides in GeSi-Si and Si-on-SiO<sub>2</sub>. *IEEE J. Quantum Electron.* 27, 1971–1974 (1991). <https://doi.org/10.1109/3.83406>
28. Pogossian, S.P., Vescan, L., Vonsovici, A.: The Single-Mode Condition for Semiconductor Rib Waveguides with Large Cross Section. *J. Light. Technol.* 16, 1851–1853 (1998). <https://doi.org/10.1109/JLT.2004.832427>
29. Ziyang, M., Li, L., Hongtao, L., Xiaowu, N.: Theoretical study of weakly-guided large-mode-area rib waveguides: single-mode condition, birefringence, and supermode generation. *Opt. Quantum Electron.* 48, (2016). <https://doi.org/10.1007/s11082-016-0828-z>
30. Solehmainen, K., Aalto, T., Dekker, J., Kapulainen, M., Harjanne, M., Heimala, P.: Development of multi-step processing in silicon-on-insulator for optical waveguide applications. *J. Opt. A Pure Appl. Opt.* 8, (2006). <https://doi.org/10.1088/1464-4258/8/7/S22>
31. Cassan, E., Laval, S., Lardenois, S., Koster, A.: On-Chip Optical Interconnects With Compact and Low-Loss Light Distribution in Silicon-on-Insulator Rib Waveguides. *IEEE J. Sel. Top. Quantum Electron.* 9, 460–464 (2003). <https://doi.org/10.1109/IITC.2003.1219706>
32. Costa, J., Almeida, D., Fantoni, A., Lourenço, P.: Performance of an a-Si:H MMI multichannel beam splitter analyzed by computer simulation. *Silicon Photonics XVI, SPIE.* 1169106, (2021). <https://doi.org/10.1117/12.2583028>
33. Vieira, M.A., Vieira, M., Louro, P., Silva, V., Costa, J., Fantoni, A.: SiC Multilayer Structures as Light Controlled Photonic Active Filters. *Plasmonics.* 8, 63–70 (2013). <https://doi.org/10.1007/s11468-012-9422-9>
34. Chute, C., French, T.: Introducing care 4.0: An integrated care paradigm built on industry 4.0 capabilities. *Int. J. Environ. Res. Public Health.* 16, (2019). <https://doi.org/10.3390/ijerph16122247>
35. Thuemmler, C., Bai, C.: Health 4.0: How virtualization and big data are revolutionizing healthcare. *Heal. 4.0 How Virtualization Big Data are Revolutionizing Healthc.* 1–254 (2017). <https://doi.org/10.1007/978-3-319-47617-9>
36. Haick, H., Tang, N.: Artificial Intelligence in Medical Sensors for Clinical Decisions. *ACS Nano.* 15, 3557–3567 (2021). <https://doi.org/10.1021/acsnano.1c00085>
37. Qazi, S., Raza, K.: Smart biosensors for an efficient point of care (PoC) health management. In: *Smart Biosensors in Medical Care.* pp. 65–85. Academic Press (2020)
38. Jiang, Y., Pillai, S., Green, M.A.: Realistic Silver Optical Constants for Plasmonics. *Sci. Rep.* 6, 1–7 (2016). <https://doi.org/10.1038/srep30605>
39. Charifi, H., Slaoui, A., Stoquert, J.P., Chaib, H., Hannour, A.: Opto-Structural Properties of Silicon Nitride Thin Films Deposited by ECR-PECVD. *World J. Condens. Matter Phys.* 06, 7–16 (2016). <https://doi.org/10.4236/wjcmp.2016.61002>